Van der Waals p–n Junction Based on an Organic–Inorganic Heterostructure

Fucai Liu, Wai Leong Chow, Xuexia He, Peng Hu, Shoujun Zheng, Xingli Wang, Jiadong Zhou, Qundong Fu, Wei Fu, Peng Yu, Qingsheng Zeng, Hong Jin Fan, Beng Kang Tay, Christian Kloc, and Zheng Liu**

Organic–inorganic heterostructures are an emerging topic that is very interesting for optoelectronics. Here, non-conventional p–n junctions are investigated using organic rubrene single crystal and 2D MoS_2 as the p- and n-type semiconducting materials, respectively. The current-rectifying behavior is clearly observed in the junction device. The rectification ratio can be electrically tuned by the gate voltage due to the 2D nature of the heterostructure. The devices also show good photoresponse properties with a photoresponsivity of ≈500 mA W^{-1} and a fast response time. These findings suggest a new route to facilitate the design of nanoelectronic and optoelectronic devices based on layered inorganics and organics.

1. Introduction

p–n junctions are essential building blocks for modern electronics and optoelectronics, including diodes, bipolar transistors, photodiodes, light-emitting diodes, and solar cells.[1,2] Conventional p–n homojunctions are formed by chemically doping a bulk semiconductor into separated p and n doping region, in order to create a graded junction region. Alternatively epitaxial growth of an n-type semiconductor on another p-type semiconductor or vice versa will form abrupt p–n junctions.[3] To ensure high quality interfaces with traditional epitaxial methods, such as pulsed laser deposition or molecular beam epitaxy, the lattice constant and crystal structure of the involved materials must be matched. This severely limits the possible material that could be utilized in such heterostructures. Recent research on graphene-like 2D materials provides us an alternative way to overcome this limitation.[4–6] The so called van der Waals heterostructures are formed by vertically stacking of different layered compounds on top of each other.[7–12] The key advantage of this method lies in a complete freedom of material choice in the hetero-stacks, due to the very weak interlayered interaction. In addition, as each layer could be freestanding, their interface will be "ideally" clean. In another words, there would be no interdiffusion of atoms at the interface, given that the transfer is conducted at room temperature. Although many fascinating physical properties have been reported from van der Waals heterostructure, its p–n junctions have not been thoroughly explored other than MoS_2/WSe_2,[13–15] MoS_2/Black phorsphorus,[16] WSe_2/carbon nanotube,[17] which are mostly inorganic materials based. Fabrication of van der Waals heterostructures based on different class of materials will reveal charming properties and new functional devices, leading to unique functionalities unachievable using conventional semiconductors.

Organic–inorganic hybrid materials combine the novel properties of inorganic solid with those of organic materials, offering the possibility to create devices with multiple functionalities.[18] For example, organic–inorganic hybrid perovskite based high efficiency solar cells and good performance photodetectors have been demonstrated.[19–22] Metal–organic frameworks are crystalline organic–inorganic hybrid materials consisting of metal ions and organic molecules, and have been intensively studied in fields of catalysis, hydrogen storage.[23] The properties of organic–inorganic hybrid can be tailored by choosing different inorganic and organic materials and compositions. 2D materials have attracted great attention due to their flexibility and unique physical properties. The marriage of inorganic 2D materials and organic ones will bring more exciting applications such as flexible electronics. In this work, we integrated MoS_2, one of the stellar materials in recent years, with rubrene, one of organic molecules which is famous for its good electric and optical properties, to form the van der Waals heterojunction and explored its photoresponse properties.

Dr. F. Liu, Dr. X. He, P. Hu, J. Zhou, Q. Fu, Dr. W. Fu, Dr. P. Yu, Dr. Q. Zeng, Prof. C. Kloc, Dr. Z. Liu
School of Materials Science and Engineering
Nanyang Technological University
Singapore 639798, Singapore
E-mail: xxhe@ntu.edu.sg; z.liu@ntu.edu.sg

W. L. Chow, X. Wang, Prof. B. K. Tay
NOVITAS, Nanoelectronics Centre of Excellent
School of Electrical and Electronic Engineering
Nanyang Technological University
Singapore 639798, Singapore

W. L. Chow, Prof. B. K. Tay, Dr. Z. Liu
CINTRA CNRS/NTU/THALES
UMI 3288, Research Techno Plaza
50 Nanyang Drive, Border X Block, Level 6
Singapore 637553, Singapore

S. Zheng, Dr. H. J. Fan
Centre for Disruptive Photonic Technologies
School of Physics and Mathematics Sciences
Nanyang Technological University
Singapore 637371, Singapore

DOI: 10.1002/adfm.201502316

Inspired by the successful isolation of graphene from graphite, transition metal dichalcogenides (TMDs) have attracted a lot of interests in recent years.[24–26] Among them, MoS_2 has attracted huge attention due to its novel electronic, optical, and optoelectronic properties.[6,27–30] MoS_2 has a layered structure and each layer is composed of a covalently bonded S–Mo–S hexagonal unit, with weak van der Waals bonding between the layers (**Figure 1**a). It is also an indirect-gap semiconductor with a band gap of 1.29 eV. When the thickness of MoS_2 is scaled down to monolayer, it becomes direct bandgap semiconductor with a bandgap of 1.9 eV and enhanced photoluminescence.[29,31] Figure 1c shows the absorption spectrum of the MoS_2 thin flakes, the absorpton peaks at around 660 and 600 nm, which corresponding to the A and B exciton peaks, respectively, can be clearly observed. In addition, the high electron mobility and valley circular dichroism of MoS_2 make it a promising candidate for future electronic, optoelectronic and valleytronic device applications.[6,28]

On the other hand, due to the high mechanical flexibility, versatile chemical design, and low-temperature processing, organic materials have also attracted a lot of interests for the applications in novel electronic and optoelectronic devices such as field-effect transistors (FETs)[32] and light-emitting diodes (LEDs).[33–35] Rubrene ($C_{42}H_{28}$) single crystal is one of the most prominent materials for the study of organic electronics because it possesses band-like transport properties with hole mobility as high as 43 $cm^2\ V^{-1}\ s^{-1}$,[36,37] and good optical properties such as high quantum efficient photoluminescence.[38,39] The molecular structure of rubrene is shown in Figure 1b. The absorption spectrum of rubrene is also shown in Figure 1d. The structure around 530 nm and the peaks (500 and 460 nm) on the higher-energy side are a zero-phonon line of the lowest exciton and its phonon side bands, respectively.[40] Stacking the n-type MoS_2 with p-type rubrene in the vertical direction enable us to form a van der Waals heterojunction p–n diode, which shows good rectifying behavior and gate-tunability. The diodes also exhibit good photoresponse with a high photoresponsivity of about 500 mA W^{-1}. The p–n heterojunction demonstrated here provides a new route for electronic and optoelectronic devices with low cost and high flexibility.

2. Results and Discussions

2.1. p–n Heterostructure Fabrication and Characterization

Before fabrication of the heterojunction p–n diodes, we first characterized the electrical transport properties of MoS_2 and rubrene in order to confirm the nearly Ohmic contacts to MoS_2 and rubrene, respectively. We first fabricated the field effect transistor of the MoS_2 and rubrene single crystal, respectively. The MoS_2 field effect transistors were fabricated using photolithography with top contact geometry. **Figure 2**a,b

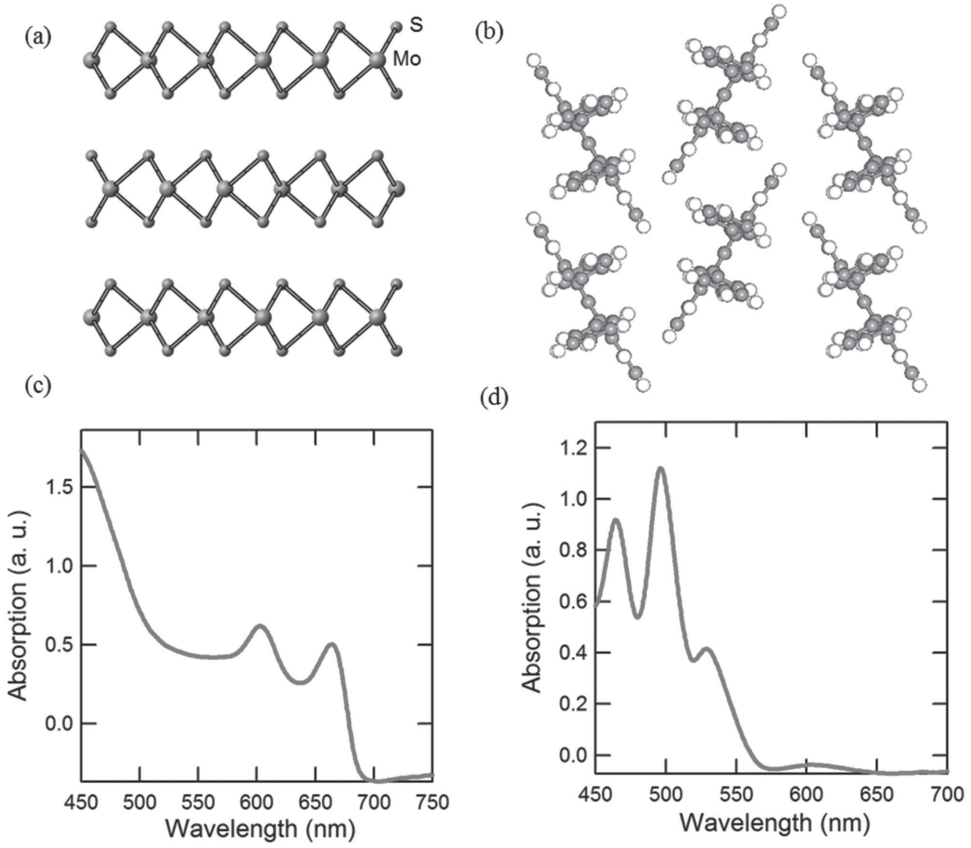

Figure 1. a) The side view of the MoS_2 crystal structure. The crystal has an interlayer van der Waals interaction and hexagonal in-plane structure. b) Molecular structure of rubrene corresponding projection on the ab plane. The absorption spectrum of c) MoS_2 and d) rubrene. A and B exciton peaks are clearly observed in MoS_2. The peaks in (d) correspond to the exciton absorption of rubrene and its phonon side bands.

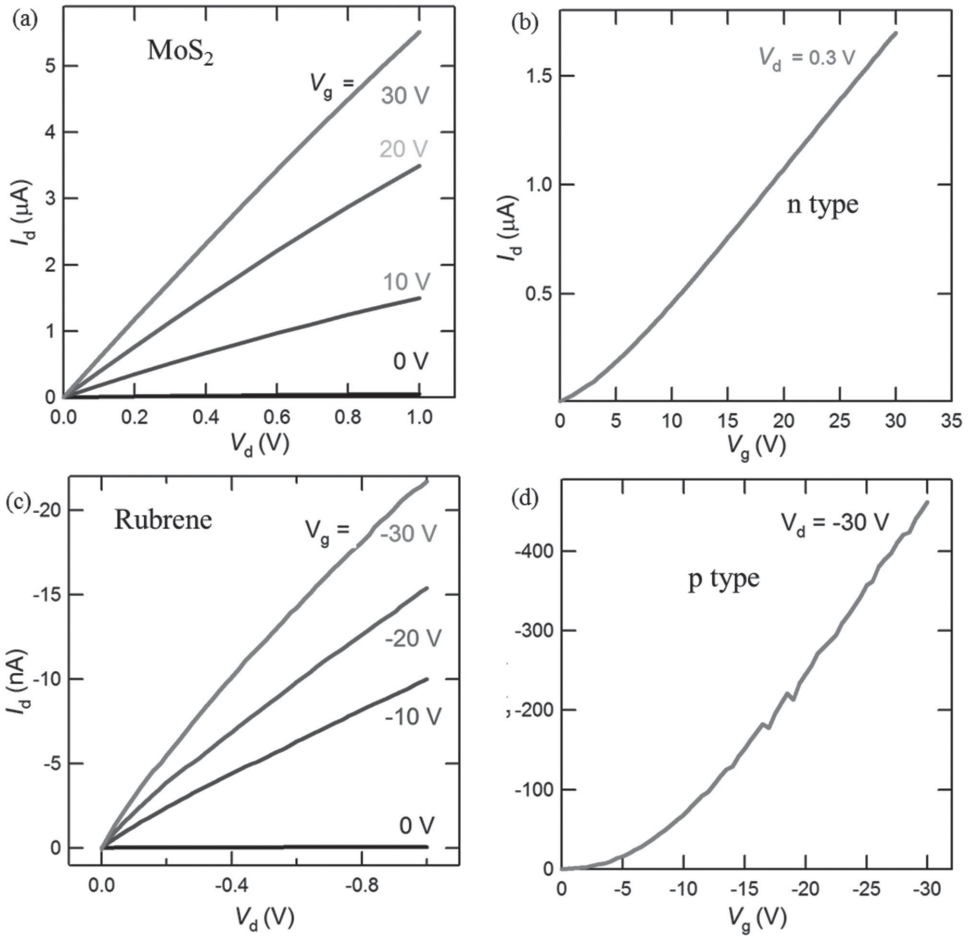

Figure 2. a) The output and b) transfer curve of the MoS_2 field effect transistor. The nearly linear I_d–V_d curve in low voltage range indicates negligible Schottky barrier the MoS_2/metal electrode interface. The mobility and On/Off ratio are about 8 $cm^2\ V^{-1}\ s^{-1}$ and 10^2, respectively. c) The output and d) transfer curve of the rubrene field effect transistor with bottom contact and bottom gate geometry. The device shows a typical p-type behavior. The mobility and On/Off ratio are around 0.1 $cm^2\ V^{-1}\ s^{-1}$ and 10^3, respectively.

shows the typical output and transfer curves, respectively. The field-effect mobility of this device was estimated from the linear region in the I_d–V_g curve by using the equation $\mu = \frac{dI_d}{dV_g} \times \frac{L}{WC_iV_d}$, where L is the channel length, W is the channel width, and C_i is the capacitance between the channel and the back gate per unit area ($C_i = \varepsilon_0\varepsilon_r/d$; ε_0 is the vacuum permittivity, ε_r is the relative permittivity, and d is the thickness of SiO_2 layer). The devices show a typical n-type behavior with electron mobility in the range 1–10 $cm^2\ V^{-1}\ s^{-1}$, which is consistent with previous reports.[41,42] The device shown in Figure 2a,b has a mobility of about 8 $cm^2\ V^{-1}\ s^{-1}$. When the gate voltage was varied from 30 to 0 V, a drop in drain current by a factor of 2×10^2 was observed. The relatively low On/Off ratio and high Off current at gate voltage of 0 V is due to the n-type doping nature of MoS_2, By applying high negative gate voltage, the On/Off ratio can be increased.[42] The rubrene FET was fabricated by laminating rubrene single crystal on the fabricated gold electrode, forming bottom contacts and bottom gate geometry. The output and transfer curve is shown in Figure 2c,d. A p-type operation behavior is observed for rubrene FET.[43,44] The mobility and On/Off ration of rubrene transistor were deduced to be about 0.1 $cm^2\ V^{-1}\ s^{-1}$ and 10^3, respectively. The nearly linear I_d–V_d curve in low drain current range of both MoS_2 and rubrene devices indicating a very low contact resistance between Au and MoS_2 or rubrene, which is importance for the fabrication of high performance p–n junction.

The fabrication process of the MoS_2/rubrene heterojunction is as follows. First, we mechanically exfoliated the MoS_2 thin flakes on the degenerately doped Si substrate covered with 285 nm thick SiO_2 using standard scotch tape method[45] (**Figure 3**a,d,g). The geometries and thickness of the thin flakes were identified using optical microscopy and atomic force microscopy. The MoS_2 with a thickness of about 5 nm (inset of Figure 3g) which has relatively large lateral size are selected for the heterostructure fabrication. After locating the MoS_2 flakes under microscope, electrodes were patterned using photolithography. The source electrode is conducted to MoS_2 flake while the drain electrode is away from it (Figure 3b,e,h). Finally, rubrene single crystals were picked up and carefully positioned between the MoS_2 and the drain electrode under microscope (Figure 3c,f,i). The typical thickness of rubrene crystal is around 300 nm (inset of Figure 3i). The hetetrojunction will then be formed between the overlapped region of MoS_2 and rubrene.

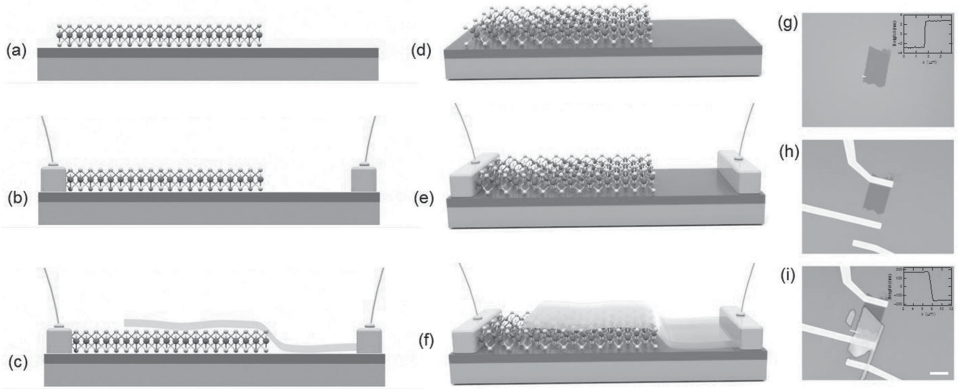

Figure 3. a–c) Side view and d–f) top view, and g–i) typical optical images of the fabrication process of the p–n junction fabrication process. a,d,g) MoS_2 thin fakes are exfoliated on the surface of Si/SiO_2 substrate using scotch tape method. b,e,h) Gold electrode is patterned on top of MoS_2 flake using traditional photolithography process, with one side contact to MoS_2 and the other side away from it. c,f,i) The rubrene single crystal is picked up and placed between the MoS_2 flake and the gold electrode under optical microscopy, the overlap range formed the heterojunction. The scale bar in (i) is 20 μm. The color difference of substrates in (g–i) is due to the different exposue times. The inset of Figure g and i show the height profile of MoS_2 and rubrene, with thickness of 5 and 300 nm, respectively.

Electrical transport characterizations of the heterojunction p–n diode are performed as shown in **Figure 4**a. The device shows standard p–n diode characteristics with a clear rectifying behavior, with current only being able to pass through the device when the p-type rubrene is positively biased. The strong current-rectifying characteristic indicates a good van der Waals p–n heterojunction formed between n-type layered MoS_2 and p-type rubrene thin semiconductors.

Due to the ultrathin nature of the MoS_2 layer, the electrical characteristics of the van der Waals diode can be easily tuned by the back gate. Figure 4a presents the I_d–V_d curves of the junction at various gate voltages. We observed gate voltage-tuned rectification of current as electrostatic doping modulates the density of free electrons and holes in the junction. As can be seen from Figure 4b, both the current under forward and reverse biased conditions can be effectively tuned by the gate voltage. The transfer characteristics of the junction show unusual gate voltage dependence. The drain current starts to increase when applying the negative gate voltage, and achieves a maximum at gate voltage of about −20 V. Then the drain voltage decreased dramatically while keeping increase the gate voltage, which is different from conventional behavior of field effect transistor. This behavior can be explained as originated from an FET channel consisting of two p and n semiconductors in series. Due to the low hole density of organic material, the sheet resistance of rubrene is much larger than exfoliated MoS_2, and the conductivity of the device is dominated by the rubrene channel. MoS_2 is usually n doped induced by the S vacancies and has a lot of electrons,[46] which has higher conductivity than rubrene. Under positive gate voltage, the holes in rubrene are depleted due to the gating and the device is under OFF state. When the device is negatively gated, the hole accumulates in the rubrene layer, leading to an increasing current for the whole junction. When the voltage is high enough, the electrons in MoS_2 is fully depleted. Therefore, the current through the junction is dominated by the MoS_2 layer, which decreases after a higher negative gating voltage (> −10 V) was applied.

An important parameter in characterizing diode characteristics is the rectifying ratio, which is the ratio of the forward current to the reverse current at the same bias magnitude. Figure 4c shows that the ratio varies from 10^2 to 10^5 as a function of gate voltage, which is much larger than that of MoS_2/WSe_2 junction.[14,15] This value is also comparable to the one from inorganic MoS_2-black phosphorus junction.[16] The gate modulation of the rectifying ratio is attributed to the modulation of band alignment of MoS_2 and rubrene by the back gating, as

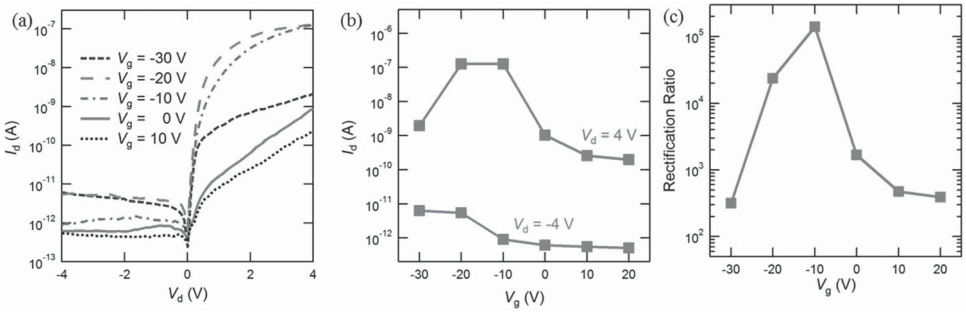

Figure 4. a) The I_d–V_d curve of the MoS_2-rubene p–n junction under different gate voltage. Typical rectifying behavior is observed. b) The drain current change as a function of the gate voltage under forward and reverse biased condition extract from (a). Both the current at forward and reverse biased condition can be effectively modulated by the gate voltage. c) The rectifying ratio as a function of the gate voltage extracted from (b). The ratio can be tuned from 10^2 to 10^5.

well as the sheet resistance modulation. We have also fitted the diode characteristics and calculated the ideality factor of our heterojunction device based on the model of a p–n diode with a series resistor. The ideal factor is deduced to be 3.9 and is similar to the junction based on MoS_2-black phosphorus junction. It is slightly larger than the electrically tunable p–n WSe_2 diodes,[13] which can be attributed to large trap densities at the interfaces.[16]

2.2. Characterization of Photoresponse Properties

Both MoS_2 and rubrene exhibit good optical properties like large excitonic absorption and PL, which shed a light on a high-performance p–n junction for optoelectronic applications. Generally, when the excitation photon energy is larger than the bandgap of MoS_2 and rubrene, the electrons can be excited from the valence band to the conduction band. Photocurrent can be generated. In order to evaluate its performance, we use a 532 nm semiconductor laser, which can excite the carriers both in MoS_2 and rubrene, as the illumination source to investigate the photoresponse properties of the heterostructure. We first investigated the light intensity dependence of the photocurrent. As can be seen from **Figure 5**a, by increasing the laser intensity, the photocurrent changed dramatically. Figure 5b plots the photocurrent as a function of light intensity under different drain voltages. The generation of the photocurrent can be explained in the following way: as shown in the inset of Figure 5b, the photogenerated electron–hole pairs were firstly separated at the overlapped p–n junction region. Therefore, it moved to the source and drain electrodes under the driven of drain bias and generated photocurrent. By increasing the light intensity, more electron–hole pairs were generated and separated, resulting in the light intensity dependence of the photocurrents.

One of the most important parameters for a photodetector is its photoresponsivity *R*, which is the ratio of generated photocurrent to the intensity of the incident light. The photoresponsivity of the p–n junction under drain voltage of 4 V and light intensity of 20 mW cm^{-2} is calculated to be 510 mA W^{-1}, which is several times higher than previously report heterostructures based on MoS_2-carbon nanotube,[17] and WSe_2 homojunction.[13,15,47] Such high responsivity reported here will pave the way for the new generation optoelectronic devices using hybrid inorganic–organic structure.

The strong photoresponse properties allow the application of the p–n junction as a photodetector. Usually, the photoresponse time is one of the key parameters for the photodetector. The time-resolved response of the photodetector was carried out by mechanically modulating the intensity of the incoming light and recording the current under drain voltage of 5 V. The time dependent photoresponse is presented in **Figure 6**a. By switching the illumination on and off alternatively, the photocurrent changes accordingly. The On and Off current states for each cycle shown here remain almost constant within the noise level, indicating the reversibility and stability of the junction over this time interval. Figure 6b,c shows the temporal evolution of the photocurrent just after the laser was switched on or off, respectively. The response time is less than 5 ms (beyond the resolution of our system), suggesting the fast response of the device. Due to the p–n junction nature of the device, much faster response is expected by improving the time resolution of the measurement system.

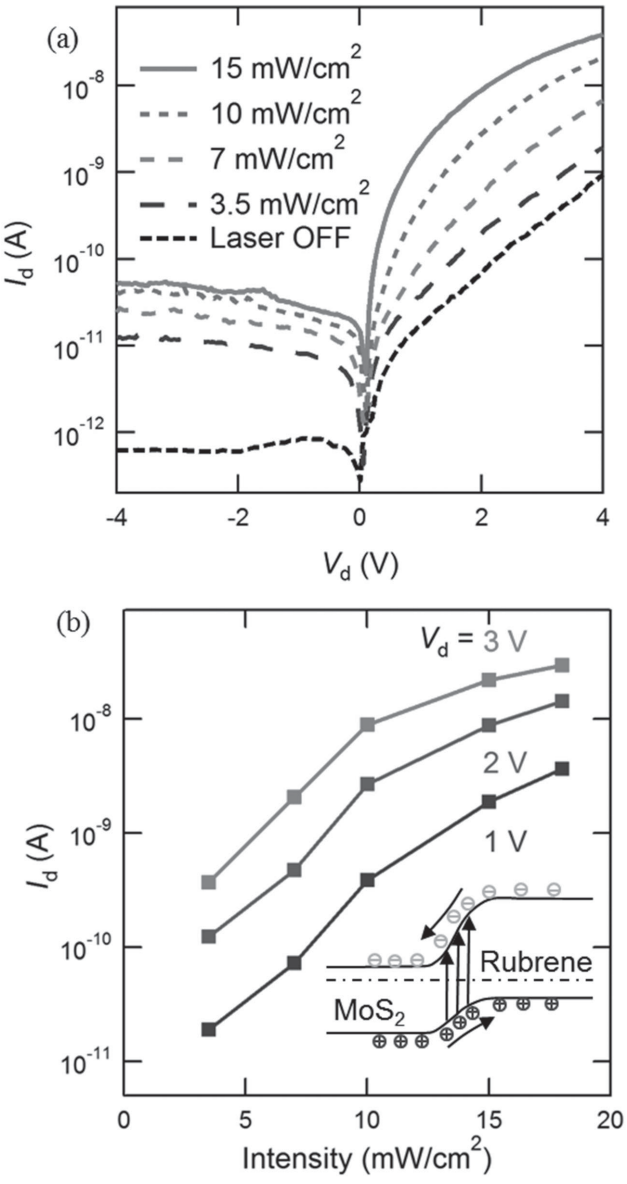

Figure 5. a) The drain current change as a function of drain voltage under different light intensity excitation. b) Photocurrent as a function of incident laser intensity under different drain voltage. Increasing the illumination intensity results in the increase of photocurrent. The inset shows the schematic for the photocurrent generation process of the p–n junction under light illumination.

3. Conclusion

In summary, we have fabricated the van der Waals heterojunction based on inorganic n-type MoS_2 and organic p-type rubrene. The p–n diode showed good current rectifying characteristics, and can be controlled by the gate voltage due to ultrathin nature of MoS_2

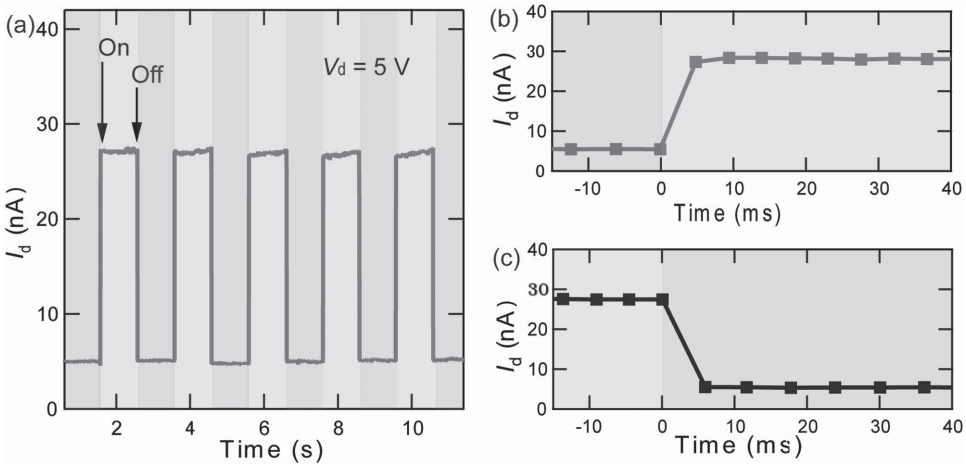

Figure 6. a) The switch behavior of the p–n junction under the light illumination on and off alternatively. The time resolved photocurrent change just after the light is switched b) On and c) Off is shown. The device can be switched between On and Off state within 5 ms.

layer. The rectifying ratio can be modulated from 10^2 to 10^5. Good photoresponse properties were also observed with a high photoresponsivity and fast response time. Very recently, monolayer organic crystals has been synthesized,[48] the marriage of various 2D organic materials with increasing families of 2D inorganic materials will open up new opportunities for novel electronic and optoelectronic device such as Ultimate thin vertical p–n junction based on monolayer inorganic and organic crystals.[49]

4. Experimental Section

MoS_2 thin flakes were exfoliated from single crystal (SPI) by using scotch tape method. Identification of the thin flakes was performed using optical microscope and atomic force microscopy. The rubrene single crystals were grown via physical vapor transport method. The thickness of the MoS_2 and rubrene flakes was measured by atomic force microscopy (Cypher S, Asylum Research). The absorption spectra were recorded using Jasco MSV-5200 microscopic spectrophotometer. Electrodes are patterned using photolithography followed by thermal evaporation and lift off process. Electric measurements were conducted in ambient conditions using a semiconductor parameter analyzer (Agilent, B1500A). A semiconductor laser with a wavelength of 532 nm was used to study the photoresponse properties of the devices.

Acknowledgements

F.L and W.L.C. contributed equally to this work. This work was supported by the Singapore National Research Foundation under NRF RF Award No. NRF-RF2013–08, the start-up funding from Nanyang Technological University (M4081137.070), NTU-A*STAR Silicon Technologies Centre of Excellence under the Program Grant No. 11235100003, Singapore Ministry of Education Academic Research Fund Tier 1 (RG10/14) and MOE Tier 3 (Grand No. MOE2011-T3-1-005).

Received: June 7, 2015
Revised: July 26, 2015
Published online: August 18, 2015

[1] M. Buscema, D. J. Groenendijk, G. A. Steele, H. S. van der Zant, A. Castellanos-Gomez, *Nat. Commun.* **2014**, *5*, 4651.
[2] Y. Taniyasu, M. Kasu, T. Makimoto, *Nature* **2006**, *441*, 325.
[3] F. Ponce, D. Bour, *Nature* **1997**, *386*, 351.
[4] L. Li, Y. Yu, G. J. Ye, Q. Ge, X. Ou, H. Wu, D. Feng, X. H. Chen, Y. Zhang, *Nat. Nanotechnol.* **2014**, *9*, 372.
[5] K. S. Novoselov, A. K. Geim, S. Morozov, D. Jiang, Y. Zhang, S. V. Dubonos, I. V. Grigoieva, A. A. Firov, *Science* **2004**, *306*, 666.
[6] B. Radisavljevic, A. Radenovic, J. Brivio, V. Giacometti, A. Kis, *Nat. Nanotechnol.* **2011**, *6*, 147.
[7] L. Britnell, R. Ribeiro, A. Eckmann, R. Jalil, B. Belle, A. Mishchenko, Y.-J. Kim, R. V. Gorbachev, T. Georgiou, S. V. Morozov, A. N. Grigorenko, A. K. Geim, C. Casiraghi, A. H. Castro Neto, K. S. Novoselov, *Science* **2013**, *340*, 1311.
[8] H. Fang, C. Battaglia, C. Carraro, S. Nemsak, B. Ozdol, J. Kang, H. A. Bechtel, S. Desai, F. Kronast, A. A. Unal, G. Conti, C. Conlon, G. K. Palsson, M. C. Martin, A. M. Minor, C. S. Fadley, E. Yablonovitch, R. Maboudian, A. Javey, *Proc. Natl. Acad. Sci. USA* **2014**, *111*, 6198.
[9] X. Hong, J. Kim, S.-F. Shi, Y. Zhang, C. Jin, Y. Sun, S. Tongay, J. Wu, Y. Zhang, F. Wang, *Nat. Nanotechnol.* **2014**. *9*, 682.
[10] B. Hunt, J. Sanchez-Yamagishi, A. Young, M. Yankowitz, B. LeRoy, K. Watanabe, T. Taniguchi, P. Moon, M. Koshino, P. Jarillo-Herero, R. C. Ashori, *Science* **2013**, *340*, 1427.
[11] L. Ju, J. Velasco Jr., E. Huang, S. Kahn, C. Nosiglia, H. Tsai, W. Yang, T. Taniguchi, K. Watanabe, Y. Zhang, G. Zhang, M. Crommie, A. Zettl, F. Wang, *Nat. Nanotechnol.* **2014**, *9*, 348.
[12] A. Geim, I. Grigorieva, *Nature* **2013**, *499*, 419.
[13] B. W. Baugher, H. O. Churchill, Y. Yang, P. Jarillo-Herrero, *Nat. Nanotechnol.* **2014**, *9*, 262.
[14] R. Cheng, D. Li, H. Zhou, C. Wang, A. Yin, S. Jiang, Y. Liu, Y. Chen, Y. Huang, X. Duan, *Nano Lett.* **2014**, *14*, 5590.
[15] M. M. Furchi, A. Pospischil, F. Libisch, J. Burgdörfer, T. Mueller, *Nano Lett.* **2014**, *14*, 4785.
[16] Y. Deng, Z. Luo, N. J. Conrad, H. Liu, Y. Gong, S. Namjmaei, P. Ajayan, J. Lou, X. Xu, P. D. Ye, *ACS Nano* **2014**, *8*, 8292.
[17] D. Jariwala, V. K. Sangwan, C.-C. Wu, P. L. Prabhumirashi, M. L. Geier, T. J. Marks, L. J. Lauhon, M. C. Hersam, *Proc. Natl. Acad. Sci. USA* **2013**, *110*, 18076.
[18] C. Kagan, D. Mitzi, C. Dimitrakopoulos, *Science* **1999**, *286*, 945.
[19] M. Liu, M. B. Johnston, H. J. Snaith, *Nature* **2013**, *501*, 395.
[20] H. Zhou, Q. Chen, G. Li, S. Luo, T.-B. Song, H. Duan, Z. Hong, J. You, Y. Liu, Y. Yang, *Science* **2014**, *345*, 542.
[21] L. Dou, Y. M. Yang, J. You, Z. Hong, W.-H. Chang, G. Li, Y. Yang, *Nat. Commun.* **2014**, *5*, 5404.
[22] X. Hu, X. Zhang, L. Liang, J. Bao, S. Li, W. Yang, Y. Xie, *Adv. Funct. Mater.* **2014**, *24*, 7373.
[23] S. L. James, *Chem. Soc. Rev.* **2003**, *32*, 276.
[24] Q. Wang, K. Kalantra-Zadh, A. Kis, J. Coleman, M. Strano, *Nat. Nanotechnol.* **2012**, *7*, 699.

[25] M. Xu, T. Liang, M. Shi, H. Chen, *Chem. Rev.* **2013**, *113*, 3766.
[26] D. Jariwala, V. K. Sangwan, L. J. Lauhon, T. J. Marks, M. C. Hersam, *ACS Nano* **2014**, *8*, 1102.
[27] K. F. Mak, K. He, C. Lee, G. H. Lee, J. Hone, T. F. Heinz, J. Shan, *Nat. Mater.* **2013**, *12*, 207.
[28] K. F. Mak, K. He, J. Shan, T. F. Heinz, *Nat. Nanotechnol.* **2012**, *7*, 494.
[29] K. F. Mak, C. Lee, J. Hone, J. Shan, T. F. Heinz, *Phys. Rev. Lett.* **2010**, *105*, 136805.
[30] H. Zeng, J. Dai, W. Yao, D. Xiao, X. Cui, *Nat. Nanotechnol.* **2012**, *7*, 490.
[31] G. Eda, H. Yamaguchi, D. Voiry, T. Fujita, M. Chen, M. Chhowalla, *Nano Lett.* **2011**, *11*, 5111.
[32] C. Reese, Z. Bao, *Mater. Today* **2007**, *10*, 20.
[33] R. Capelli, S. Toffanin, G. Generali, H. Usta, A. Facchetti, M. Muccini, *Nat. Mater.* **2010**, *9*, 496.
[34] F. Cicoira, C. Santato, *Adv. Funct. Mater.* **2007**, *17*, 3421.
[35] M. McCarthy, B. Liu, E. Donoghue, I. Kravchenko, D. Kim, F. So, A. G. Rinzler, *Science* **2011**, *332*, 570.
[36] V. Podzorov, E. Menard, A. Borissov, V. Kiryukhin, J. Rogers, M. Gershenson, *Phys. Rev. Lett.* **2004**, *93*, 086602.
[37] V. C. Sundar, J. Zaumseil, V. Podzorov, E. Menard, R. L. Willett, T. Someya, M. E. Grshenson, J. A. Rogers, *Science* **2004**, *303*, 1644.
[38] O. Mitrofanov, D. V. Lang, C. Kloc, J. M. Wikberg, T. Siegrist, W. So, M. A. Sergent, A. P. Ramirez, *Phys. Rev. Lett.* **2006**, *97*, 166601.
[39] H. Najafov, B. Lee, Q. Zhou, L. Feldman, V. Podzorov, *Nat. Mater.* **2010**, *9*, 938.
[40] S. Tavazzi, A. Borghesi, A. Papagni, P. Spearman, L. Silvestri, A. Yassar, A. Camposeo, M. Polo, D. Pisignano, *Phys. Rev. B* **2007**, *75*, 245416.
[41] A. Ayari, E. Cobas, O. Ogundadegbe, M. S. Fuhrer, *J. Appl. Phys.* **2007**, *101*, 014507.
[42] S. Kim, A. Konar, W.-S. Hwang, J. H. Lee, J. Lee, J. Yang, C. Jung, H. Kim, J. Yoo, J. Choi, Y. Jin, S. Lee, D. Jena, W. Choi, K. Kim, *Nat. Commun.* **2012**, *3*, 1011.
[43] A. L. Briseno, R. J. Tseng, M. M. Ling, E. H. Falcao, Y. Yang, F. Wudl, Z. Bao, *Adv. Mater.* **2006**, *18*, 2320.
[44] A. L. Briseno, S. C. Mannsfeld, M. M. Ling, S. Liu, R. J. Tseng, C. Reese, M. E. Roberts, Y. Yang, F. Wudl, Z. Bao, *Nature* **2006**, *444*, 913.
[45] K. Novoselov, D. Jiang, F. Schedin, T. Booth, V. Khotkevich, S. V. Morozov, A. K. Geim, *Proc. Natl. Acad. Sci. USA* **2005**, *102*, 10451.
[46] H. Qiu, T. Xu, Z. Wang, W. Ren, H. Nan, Z. Ni, Q. Chen, S. Yuan, F. Miao, F. Song, G. Long, Y. Shi, L. Sun, J. Wang, X. Wang, *Nat. Commun.* **2013**, *4*, 2642.
[47] J. S. Ross, P. Klement, A. M. Jones, N. J. Ghimire, J. Yan, D. G. Mandrus, T. Taniguchi, K. Watanabe, K. Kitamura, W. Yao, D. H. Cobden, X. Xu, *Nat. Nanotechnol.* **2014**, *9*, 268.
[48] D. He, Y. Zhang, Q. Wu, R. Xu, H. Nan, J. Liu, J. Yao, Z. Wang, S. Yuan, Y. Li, Y. Shi, J. Wang, Z. Ni, L. He, F. Miao, F. Song, H. Xu, K. Watanabe, T. Taniguchi, J. Xu, X. Wang, *Nat. Commun.* **2014**, *5*, 5162.
[49] H. Li, D. Lee, D. Qu, X. Liu, J. Ryu, A. Seabaugh, W. Yoo, *Nat. Commun.* **2015**, *6*, 6564.